



Oxidative stress generated by irradiation of a zinc(II) phthalocyanine induces a dual apoptotic and necrotic response in melanoma cells

Federico Valli¹ · María C. García Vior² · Leonor P. Roguin¹ · Julieta Marino¹

Published online: 2 January 2019
© Springer Science+Business Media, LLC, part of Springer Nature 2019

Abstract

Melanoma is an aggressive form of skin carcinoma, highly resistant to traditional therapies. Photodynamic therapy (PDT) is a non-invasive therapeutic procedure that can exert a selective cytotoxic activity toward malignant cells. In this work we evaluated the effect of a cationic zinc(II) phthalocyanine (Pc13) as photosensitizer on a panel of melanoma cells. Incubation with Pc13 and irradiation induced a concentration and light dose-dependent phototoxicity. In order to study the mechanism underlying Pc13-related cell death and to compare the effect of different doses of PDT, the most sensitive melanoma B16F0 cells were employed. By confocal imaging we showed that Pc13 targeted lysosomes and mitochondria. After irradiation, a marked increase in intracellular reactive oxygen species was observed and a complete protection from Pc13 phototoxicity was reached in the presence of the antioxidant trolox. Acridine orange/ethidium bromide staining showed morphological changes indicative of both apoptosis and necrosis. Biochemical hallmarks of apoptosis, including a significant decrease in the expression levels of Bcl-2, Bcl-xL and Bid and mitochondrial membrane permeabilization, were observed at short times post irradiation. The consequent release of cytochrome *c* to cytosol and caspase-3 activation led to PARP-1 cleavage and DNA fragmentation. Simultaneously, a dose dependent increase of lactate dehydrogenase in the extracellular compartment of treated cells revealed plasma membrane damage characteristic of necrosis. Taken together, these results indicate that a dual apoptotic and necrotic response is triggered by Pc13 PDT-induced oxidative stress, suggesting that combined mechanisms of cell death could result in a potent alternative for melanoma treatment.

Keywords Reactive oxygen species · Cationic phthalocyanine · Mitochondrial membrane permeabilization · Apoptosis · Necrosis · Photodynamic therapy

Abbreviations

AO Acridine orange
DCFH-DA 2',7'-Dichlorodihydrofluorescein diacetate
DiOC₆ 3,3'-Dihexyloxacarbocyanine iodide
EB Ethidium bromide

Trolox 6-Hydroxy-2,5,7,8-tetramethylchroman-2-carboxylic acid
LDH Lactate dehydrogenase
LMP Lysosomal membrane permeabilization
 $\Delta\psi_m$ Mitochondrial transmembrane potential
Pc Phthalocyanine
PDT Photodynamic therapy
PS Photosensitizer
PARP-1 Poly(ADP-ribose) polymerase
PI Propidium iodide
ROS Reactive oxygen species
¹O₂ Singlet oxygen

Electronic supplementary material The online version of this article (<https://doi.org/10.1007/s10495-018-01512-w>) contains supplementary material, which is available to authorized users.

✉ Julieta Marino
jmarino@qb.ffyb.uba.ar

¹ Departamento de Química Biológica, Facultad de Farmacia y Bioquímica, Instituto de Química y Fisicoquímica Biológicas (IQUIFIB), Universidad de Buenos Aires, CONICET-UBA, Junín 956, C1113AAD Buenos Aires, Argentina

² Departamento de Química Orgánica, Facultad de Farmacia y Bioquímica, Universidad de Buenos Aires, CONICET, Junín 956, C1113AAD Buenos Aires, Argentina

Introduction

Melanoma is an aggressive form of skin carcinoma, resulting from malignant transformation of melanocytes. According to the International Agency for Research on Cancer,

the incidence of melanoma has been increasing in the last decades and although it represents only 5% of skin cancer, it is responsible for more than 80% of skin cancer deaths [1–3]. More than 50% of metastatic melanomas carry activating BRAF^{V600} mutations [4], whereas approximately 25% harbor mutations in NRAS [5]. Surgery and chemotherapy are effective therapeutic options when melanoma is early diagnosed. In the case of advanced-stage melanoma, clinical treatments have improved considerably with the development of immune checkpoint inhibitors and targeted therapy, such as PDL-1 blockage and BRAF and MEK inhibitors [6–8]. Despite the encouraging clinical results of novel therapies, the prognosis is poor and dependent on patient mutations and characteristics of the primary lesion including thickness, involvement of lymph nodes and propensity of malignant cells to colonize distant tissues [9]. Moreover, effectiveness of clinical use of PD-1 immune checkpoint blockade or BRAF and MEK inhibitors therapy is limited by a high rate of innate or acquired resistance in advanced metastatic melanoma [10, 11].

Photodynamic therapy (PDT) is a minimally invasive therapeutic procedure that can exert a selective cytotoxic activity toward malignant cells [12, 13]. The procedure involves the administration of a nontoxic drug or dye known as photosensitizer (PS), followed by local illumination with visible light (ideally in the red to near-infrared spectral region), which in the presence of oxygen, leads to the generation of reactive oxygen species (ROS) and consequently to cell death [14, 15]. It has been demonstrated that there are three main mechanisms by which PDT could mediate tumour destruction [16]. ROS generated by PS irradiation can kill tumour cells directly or may also damage the tumour-associated vasculature, leading to tumour infarction. Additionally, PDT can activate an immune response against tumour cells, which would be important in metastatic disease [13, 15, 17, 18].

PDT has been studied in the treatment of both premalignant and malignant tumours [19–21], including cutaneous malignancies [22]. Photofrin or aminolevulinic acid (ALA) and its derivatives has been approved for treatment of non-melanoma skin cancers, such as basal cell carcinoma (BCC) and Bowen's disease [23, 24]. Although this technique has been evaluated for melanoma, its use has shown limited success [25, 26]. This prompted the search for new photosensitizers with an increased potency, specificity for target tissues and a more effective penetration in the skin. Phthalocyanines are second generation PS that exhibit chemical stability, high yields of ROS generation, short skin photosensitivity and good spectroscopic properties (absorbance bands between 600 and 800 nm), which allow its activation in deep tissues, as penetration of light increases with wavelength [27–30].

The synthesis and photophysical characterization of the cationic zinc(II) phthalocyanine

2,9(10),16(17),23(24)-tetrakis[(2-trimethylammonium)ethylsulfanyl]phthalocyaninatozinc(II) tetraiodide (Pc13) was previously described [31]. In order to evaluate Pc13 PDT efficacy for melanoma treatment, in the present work we employed cell lines with different genotypic and phenotypic characteristics. Pc13 phototoxicity was demonstrated in all the melanoma cells assayed, being B16F0 the most sensitive cell line. Then, we investigated the mechanism underlying Pc13 related cell death in B16F0 cells and compared the effect of different doses of PDT (PS concentrations and light doses) in the extent and type of response. We also explored the organelle specificity of Pc13 and the initial events of photodamage induced after irradiation. In this sense, it has been reported that the intracellular localization of the PS plays a significant part in the fate of the cell, considering that ¹O₂ is highly reactive with a lifetime in the order of ~10–320 ns and a maximum action radius of about 10–55 nm in cells [32, 33]. Our findings revealed that Pc13 targeted both lysosomes and mitochondria of B16F0 melanoma cells and that irradiation produced a significant increase of intracellular ROS. As a result of oxidative stress, modification in the expression level of Bcl-2, Bcl-xL and Bid, mitochondrial membrane depolarization and the consequent cytochrome *c* release induced a rapid activation of the executioner caspase-3 and the cleavage of the nuclear enzyme responsible of DNA damage repair, poly(ADP-ribose) polymerase (PARP-1). The appearance of distinctive signs of necrosis after irradiation of B16F0 cells treated with Pc13 is also described in the present work. Although previous reports have shown either the induction of apoptosis or necrosis after photodynamic therapy, the simultaneous occurrence of both modes of cell death has not been demonstrated in melanoma cells. The study of a second generation photosensitizer, that targets both mitochondria and lysosomes and kills cancer cells by apoptosis and necrosis even at low PDT doses, has potential clinical relevance for melanoma treatment.

Materials and methods

Chemicals

Synthesis and purification of the sulfur-linked cationic 2,9(10),16(17),23(24)-tetrakis[(2-trimethylammonium)ethylsulfanyl]phthalocyaninatozinc(II) tetraiodide, named Pc13, has been previously described [31]. Monoclonal anti-Bax antibody, polyclonal antibodies against Bcl-2, Bcl-xL, Bid, caspase-3 and PARP were obtained from Santa Cruz Biotechnology (Santa Cruz, CA). Mouse monoclonal antibody directed against cytochrome *c* was from BD Biosciences Pharmingen (San Diego, CA) and monoclonal antibody against alpha-tubulin was purchased from Abcam

(UK). Secondary antibodies anti-mouse IgG (horseradish peroxidase-conjugated goat IgG) or anti-rabbit IgG (horseradish peroxidase-conjugated goat IgG) were from Santa Cruz Biotechnology, CA, USA. The fluorescent dyes LysoTracker and MitoTracker Green FM were obtained from Invitrogen (San Diego, CA) and ERTracker Blue-White DPX was from Molecular Probes®. Caspase-3 substrate Ac-DEVD-AMC was obtained from Peptide Institute Inc. (Osaka, Japan). Acridine orange (AO), propidium iodide (PI), ethidium bromide (EB), the probe 2',7'-dichlorodihydrofluorescein diacetate (DCFH-DA), the antioxidant 6-hydroxy-2,5,7,8-tetramethylchroman-2-carboxylic acid (trolox) and the fluorescent dye 3,3'-dihexyloxycarbocyanine iodide (DiOC₆) were from Sigma Chemical (St. Louis, MO). The pan inhibitor Z-VAD-FMK was from Santa Cruz Biotechnology (Santa Cruz, CA).

Cell cultures

Mouse melanoma cell lines B16F0 (ATCC CRL-6322) and B16F10 (ATCC CRL-6475), and the human lightly pigmented melanoma cells WM35 (Wistar Institute, Philadelphia, PA, USA) and M1/15 (donated by professor Andras Falus, Genetics Department, University Semmelweis, Budapest) were maintained in RPMI 1640 (Gibco BRL) containing 10% (v/v) fetal bovine serum (FBS, Gibco BRL), 2 mM L-glutamine, 50 U/ml penicillin, 50 µg/ml streptomycin and 4 mM sodium bicarbonate, in a humidified atmosphere of 5% CO₂ at 37 °C. A-375 cells (ATCC CRL-1619) were grown in DMEM F-12 medium with 10% (v/v) FBS, 2 mM L-glutamine, 50 U/ml penicillin, 50 µg/ml streptomycin and 4 mM sodium bicarbonate. Immortalized human keratinocytes HaCat were maintained in RPMI 1640 with 5% (v/v) FBS, 2 mM L-glutamine, 50 U/ml penicillin, 50 µg/ml streptomycin and 4 mM sodium bicarbonate.

Photodynamic treatment

Melanoma cells grown until ~70% confluence were incubated with different concentrations of Pc13 in culture medium containing 4% FBS. After 6 h of incubation (24 h for A-375 cells), the compound was removed and complete fresh culture medium was added. Then, cells were irradiated with a 150 W halogen lamp, equipped with a 10 mm water-filter to attenuate IR radiation and a 630 nm cut-off filter. A 675 ± 15 nm bandpass filter (CVI Melles Griot, Albuquerque, USA) was employed to obtain power output at wavelengths to which there is maximum Pc13 absorbance [31]. The total power output was 0.28 mW cm⁻², measured with a FieldMate laser power meter (Coherent, Wilsonville, USA). Light doses at 675 ± 15 nm were 170 mJ cm⁻², 340 mJ cm⁻², 680 mJ cm⁻², for 10 min, 20 min or 40 min of irradiation,

respectively. In parallel, cells incubated in the absence of Pc13 were used as control.

In some experiments, Pc13-loaded B16F0 cells were pre-incubated for 1 h before irradiation with 5 mM of the antioxidant trolox or 25 µM of the caspase pan inhibitor Z-VAD-FMK. After light exposure, cells were incubated for 24 h and phototoxicity was evaluated by MTT assay or colorimetric determination of hexosaminidase activity with p-nitro phenol substrate as previously described [34]. Absorbance values were measured in a Biotrack II Microplate Reader (GE Healthcare, Piscataway, NY).

Pc13 subcellular localization

B16F0 cells (3×10^4) grown on coverslips were incubated with a 5 µM solution of Pc13 for 24 h at 37 °C in the dark. After removing the phthalocyanine with PBS, cells were stained with the organelle specific fluorescent dyes LysoTracker Green DND-26 (100 nM, 45 min), MitoTracker Green FM (100 nM, 45 min) and ERTracker Blue-White (1 µM, 1 h) diluted in the culture medium without FBS. Then, cells were washed with PBS and fresh medium was added to examine fluorescence by confocal microscopy (Olympus FV 300). Pc13 was excited at 633 nm and its emission was monitored at wavelengths of 655–755 nm. Lysosomal and mitochondrial probes were excited at 488 nm and green fluorescence was detected at 510–530 nm, while ER probe was excited at 405 nm and its blue emission was observed at 425–475 nm.

Determination of intracellular ROS production

The endogenous ROS content was evaluated from the oxidation of the probe 2',7'-dichlorodihydrofluorescein diacetate (DCFH-DA). B16F0 cells were plated at a density of 3×10^5 cells/well in 6-well microplates and incubated overnight at 37 °C until 70–80% of confluence. Then, the culture medium was replaced by RPMI containing 4% FBS and different concentrations of Pc13. After 24 h, the compound was removed, cells were washed with PBS and incubated in the presence of 10 µM DCFH-DA at 37 °C for 20 min. Non-incorporated probe was eliminated and cells were irradiated with 340 mJ cm⁻² in medium containing 10% FBS. Cells were harvested, counted with a 0.4% solution of Trypan Blue, and then lysed with a solution of 0.1% (v/v) of Triton X-100 in PBS for 30 min. DCF green fluorescence was detected in a Jasco FP-6500 fluorometer using 485 nm excitation and 530 nm emission wavelengths. Results were expressed as DCF fluorescence per cell, relative to control.

Alternatively, DCF fluorescence of Pc13-treated cells grown on coverslips was examined with a Leica DM2000 fluorescence microscope at 470–490 nm excitation and 515 nm emission wavelengths.

Acridine orange and ethidium bromide cell staining

B16F0 cells grown on coverslips were incubated with 0.2 μM of Pc13 for 24 h in the dark. Then, cells were irradiated (340 mJ cm^{-2}) and stained with 50 $\mu\text{g/ml}$ ethidium bromide, 50 $\mu\text{g/ml}$ acridine orange at different times post irradiation (p.i.). Alternatively, Pc13-loaded B16F0 cells were pre-incubated for 1 h before irradiation with 5 mM trolox. Cell morphology and staining were examined in a Leica DM2000 fluorescence microscope. Images obtained were then analyzed and percentage of viable, apoptotic and necrotic cells was quantified.

Lactate dehydrogenase release assay

Cell membrane permeabilization was determined by the release to the medium of the cytosolic enzyme LDH using the LDH-P UV AA kit (Wiener lab., Rosario, Argentina), according to the manufacturer's protocol [35]. Briefly, B16F0 cells (5×10^5 cell/well) seeded in 6-well plates were incubated overnight with different concentrations of Pc13 and after washing with PBS and irradiating with 340 mJ cm^{-2} or 680 mJ cm^{-2} , 20 μl of culture supernatants were employed to assess LDH activity at different times post irradiation. The decrease in 340 nm absorbance, corresponding to NADH consumption, was monitored with a Jasco V550 spectrophotometer. For maximum lysis control, cells were incubated for 1 h at room temperature with a 1% solution of Triton X-100.

Evaluation of mitochondrial membrane potential

To measure the mitochondrial membrane potential ($\Delta\psi\text{m}$), B16F0 cells pre-loaded or not with 0.2 μM Pc13 for 24 h at 37 °C in the dark, were treated with a light dose of 340 mJ cm^{-2} . Immediately after irradiation and 1 h p.i., cells were incubated with 40 nM of the potential-sensitive cationic lipophilic dye 3,3'-dihexyloxacarbocyanine iodide (DiOC_6) for 30 min at 37 °C. Green fluorescence for DiOC_6 was measured by using a FACSCalibur flow cytometer (Becton Dickinson, CA, USA).

Alternatively, B16F0 cells were grown in coverslips and cell fluorescence was monitored by a Leica DM2000 fluorescence microscope at 470–490 nm excitation and 515 nm emission wavelengths.

Western blot assays

B16F0 cells (2×10^6) were incubated during 24 h with a 0.2 μM solution of Pc13, then washed with PBS and exposed to a light dose of 340 mJ cm^{-2} in RPMI, 10% FBS. At different times post irradiation, cells were lysed for 30 min at 4 °C in 10 μl of lysis buffer (0.5% Triton X-100, 1 $\mu\text{g/}$

ml aprotinin, 1 $\mu\text{g/ml}$ trypsin inhibitor, 1 $\mu\text{g/ml}$ leupeptin, 10 mM $\text{Na}_4\text{P}_2\text{O}_7$, 10 mM NaF, 1 mM Na_3VO_4 , 1 mM EDTA, 1 mM PMSF, 150 mM NaCl, 50 mM Tris, pH 7.4). Clear supernatants were centrifuged at $17,000\times g$ for 10 min at 4 °C and protein concentration was determined using Bradford reagent. Aliquots containing 50 μg of protein were resuspended in 0.063 M Tris/HCl, pH 6.8, 2% SDS, 10% glycerol, 0.05% bromophenol blue, 5% 2-mercaptoethanol, submitted to SDS-PAGE and then transferred to PVDF membranes (GE Healthcare, Piscataway, NY) for 1 h at 100 mA per membrane (constant current) using the V20-SDB semi-dry blotting system (Scie-Plas, Cambridge, UK) in 25 mM Tris, 195 mM glycine, 20% methanol, 0.03% SDS, pH 8.2. To reduce non-specific binding, membranes were incubated for 1 h at room temperature in 10 mM Tris-HCl, 130 mM NaCl and 0.05% Tween 20, pH 7.4, (TBS-T), containing 5% non-fat milk. Membranes were then incubated overnight at 4 °C with the primary antibody, washed with TBS-T and incubated with the corresponding secondary antibody conjugated with HRP for 1 h at room temperature. Immunoreactive proteins were visualized using the ECL Plus detection system (Pierce, Thermo Scientific, Rockford, USA) according to the manufacturer's instructions. For quantification of band intensity, membranes were scanned using a densitometer (ImageQuant LAS 500, GE Healthcare Life Sciences). Equal protein loading was confirmed using a mouse anti-tubulin antibody. Band intensities were quantified using Gel-Pro Analyzer 4.1 software (Media Cybernetics).

For detection of cathepsin D and cytochrome *c* in cytosolic fraction, subcellular fractionation was performed. Briefly, B16F0 cells treated with 0.2 μM Pc13 and irradiated with a light dose of 340 mJ cm^{-2} were incubated for different time-periods at 37 °C. Cell suspensions were washed twice and incubated on ice for 15 min with sucrose buffer (250 mM sucrose, 20 mM HEPES, pH 7.5, 10 mM KCl, 1.5 mM MgCl_2 , 1 mM EDTA, 1 mM EGTA, 1 mM DTT, 0.1 mM PMSF, 1 $\mu\text{g/ml}$ aprotinin, $\mu\text{g/ml}$ leupeptin). Cells were then homogenized with a Dounce (40 strokes) and centrifuged at $1000\times g$ for 10 min at 4 °C. Supernatants were subjected to $20,000\times g$ for 20 min at 4 °C to separate lysosomal/mitochondrial fraction and the resulting supernatants were loaded onto a SDS-PAGE, transferred onto PVDF membranes and revealed with specific antibodies against cathepsin D or cytochrome *c*.

Caspase activity assay

After incubating B16F0 cells for 24 h with a 0.2 μM solution of Pc13, cells were washed and then irradiated with a light dose of 340 mJ cm^{-2} as previously described. Cells were then incubated for different time-periods at 37 °C and 1×10^6 cells were lysed for 30 min at 4 °C in 50 μl of lysis buffer

(10 mM HEPES, pH 7.4, 50 mM NaCl, 2 mM MgCl₂, 5 mM EGTA, 1 mM PMSF, 2 µg/ml leupeptin, 2 µg/ml aprotinin) followed by three cycles of rapid freezing and thawing. Cell lysates were centrifuged at 17,000×g for 15 min and total protein concentration was determined using Bradford reagent. Aliquots containing 100 µg of protein were diluted in assay buffer (20 mM HEPES, 132 mM NaCl, 6 mM KCl, 1 mM MgSO₄, 1.2 mM K₂HPO₄, pH 7.4, 20% glycerol, 5 mM DTT), and incubated at 37 °C for 1 h with 50 µM of the fluorogenic substrate for caspase-3 (Ac-DEVD-AMC). Cleavage of the substrate was monitored by AMC release in a Jasco FP-6500 fluorometer at 320 nm excitation and 400 nm emission wavelengths.

Nuclear morphology

B16F0 cells grown on coverslips at a density of 3×10^4 cells/well in a 24-well microplate were incubated in the absence (control) or presence of 0.2 µM of Pc13 for 24 h. After removing the phthalocyanine, cells were irradiated with 340 mJ cm⁻², and at different times post irradiation, cells were washed twice with PBS and fixed for 10 min at room temperature with 4% paraformaldehyde. After washing, Hoechst 33258 (2 µg/ml) was employed to stain nuclei. Images were obtained with a Leica DM2000 fluorescence microscope at 405 nm excitation and 425–460 nm emission wavelengths.

Flow cytometry analysis

B16F0 cells (6×10^5) were incubated for 24 h in the absence or presence of 0.2 µM Pc13 in the dark. After washing with PBS, cells were irradiated with a light dose of 340 mJ cm⁻². At different times post irradiation, cells were harvested, washed with cold PBS, and then fixed overnight with 1 ml of 70% cold ethanol and kept at 4 °C. Fixed cells were washed twice with PBS and resuspended in 500 µl of 0.1% sodium citrate, 0.1% Triton X-100, 50 µg/ml propidium iodide. After incubating overnight at 4 °C, the hypodiploid DNA content was analyzed in a FACSCalibur flow cytometer (Becton Dickinson, CA, USA) and percentage of hypodiploid cells was determined using Flowing software v 2.5.1. For cell cycle analysis, results were evaluated using Cylchred software (Cardiff University).

Statistical analysis

All data was presented and analyzed using GraphPad Prism (Version 6.01, GraphPad Software, La Jolla, California, USA, <http://www.graphpad.com>). Statistical analyses were performed by one-way Anova with Bonferroni post-test (comparing all groups) or Dunnett post-test (comparing all groups to a control group). Differences in values were

considered as statistically significant if p-value was less than 0.05 ($p < 0.05$). All experiments were conducted at least 3 times and expressed as mean \pm SEM, unless otherwise indicated.

Results

Phototoxic action of Pc13 in melanoma cells

The effect of cationic Pc13 (Fig. 1a) as photosensitizer was initially evaluated in the mouse melanoma cell line B16F0. While no toxicity was observed in the dark, a cytotoxic effect was achieved after irradiation of Pc13-treated cells (Fig. 1b). A marked difference in phototoxicity was observed between 170 mJ cm⁻² ($IC_{50} > 3.20$ µM) and 340 mJ cm⁻² ($IC_{50} = 0.20 \pm 0.03$ µM), corresponding to 10 and 20 min of irradiation, respectively (Fig. 1b). No considerable enhancement in Pc13 photodynamic effect was detected when light dose was increased to 680 mJ cm⁻² ($IC_{50} = 0.11 \pm 0.03$ µM). Therefore, an energy dose of 340 mJ cm⁻² was selected to perform the following characterization studies. Morphological changes reflecting cell death, including cell shrinkage, rounding and formation of vacuoles, were observed by phase contrast microscopy in Pc13-treated cells (Fig. 1c). Since an ideal PS should have no dark toxicity, we assayed the effect of higher concentrations of Pc13 without light exposure. Our results showed the absence of cytotoxicity with concentrations up to approximately $100 \times IC_{50}$ of Pc13 (Online Resource 1a).

Pc13 exerted phototoxic action in other melanoma cell lines with different genetic profile, with IC_{50} values ranging between 0.20 ± 0.03 µM (B16F0 cells) and 3.60 ± 0.23 µM (A375 cells) (Table 1, Online Resource 1b), indicating that neither the presence of melanin nor genetic background affected Pc13 PDT efficacy. Immortalized human keratinocytes (HaCat) were the less susceptible cell line with an IC_{50} value of 4.57 ± 0.20 µM (Online Resource 1c).

Pc13 selectively targets lysosomes and mitochondria

The site of photosensitizer localization has been related to the mechanism of cell death [15, 26]. Cellular internalization of Pc13 as well as its subcellular localization was determined in B16F0 cells. After incubating cells with Pc13 for 24 h, red fluorescence emission corresponding to the phthalocyanine was detected in cytoplasmic compartment by confocal microscopy (Fig. 2). In order to identify Pc13 subcellular distribution, the specific organelle probes LysoTracker Green, MitoTracker Green or ERTracker Blue-White were employed to stain lysosomes, mitochondria or endoplasmic reticulum, respectively. Overlapping of green

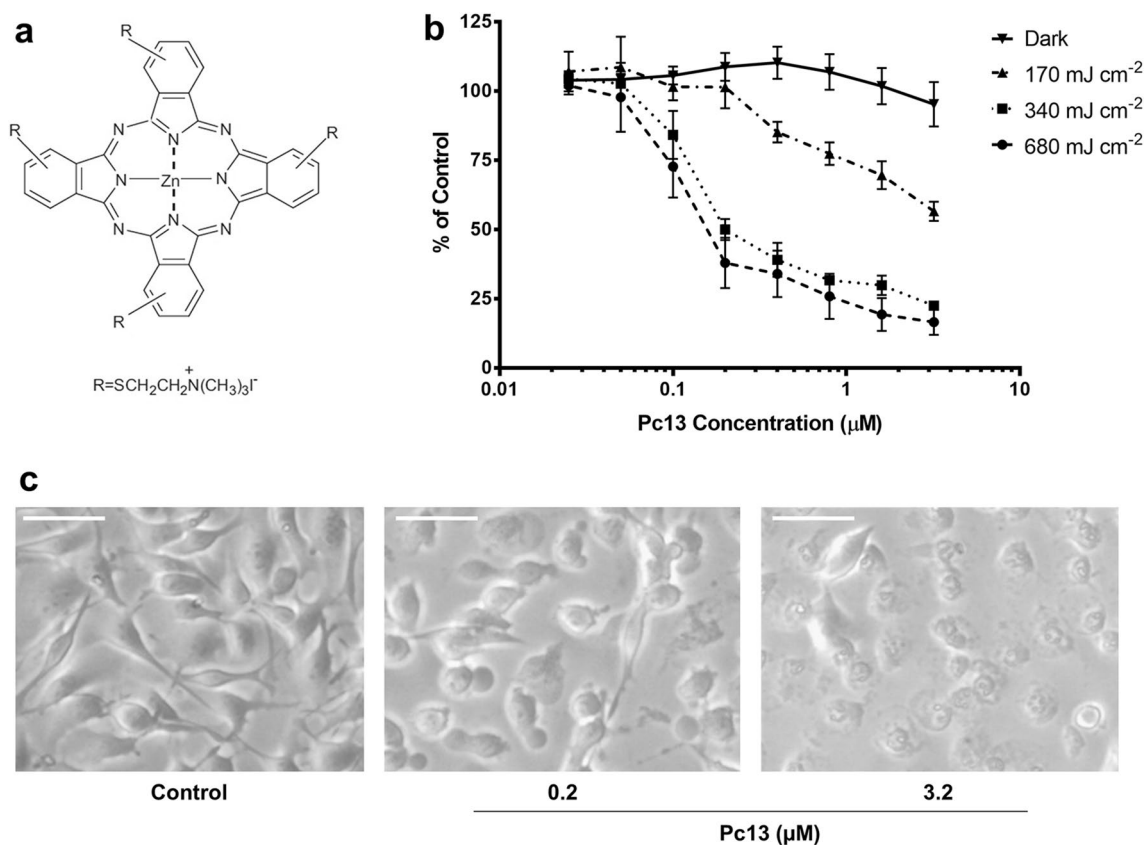


Fig. 1 Phototoxic effect of Pc13 on melanoma B16F0 cells. **a** Chemical structure of Pc13. **b** B16F0 cells incubated with different concentrations of Pc13 for 6 h were maintained in the dark or exposed to different light doses: 170 mJ cm⁻², 340 mJ cm⁻², 680 mJ cm⁻². Phototoxicity was evaluated 24 h after irradiation by MTT assay. Results are expressed relative to control obtained in the absence of

Pc13 and represent the mean \pm SEM of three different experiments. **c** Representative images of B16F0 cells captured under a phase contrast microscope (Nikon Eclipse TE300, Japan) at 3 h p.i. employing a light dose of 340 mJ cm⁻² and different concentrations of Pc13. Scale bar: 50 μ m

Table 1 Phototoxicity of Pc13 in melanoma cell lines

Cell line	Origin	Pigmented	Metastatic	BRAF	NRAS	PTEN	IC ₅₀ (μ M)
B16 F0	Murine	+	-	WT	WT	WT	0.20 \pm 0.03
B16 F10	Murine	+	+	WT	WT	WT	0.45 \pm 0.08
M1/15	Human	-	+	V600E	WT	Null	0.70 \pm 0.08
WM35	Human	Lightly	-	V600E	WT	WT	2.63 \pm 0.47
A375	Human	-	+	V600E	WT	WT	3.60 \pm 0.23

Phenotypic and genomic characteristics of different melanoma cell lines evaluated. IC₅₀ values, determined from dose–response curves, correspond to the concentration of Pc13 that inhibited 50% cell growth with a light dose of 340 mJ cm⁻². Results represent the mean \pm SEM of three different experiments

fluorescence from both LysoTracker or MitoTracker and Pc13 red fluorescence originated yellow areas, whereas no colocalization of ERTracker with Pc13 was observed, indicating that Pc13 localized partly in lysosomes and also in mitochondria (Fig. 2). These observations were quantitatively confirmed, being Pearson's correlation coefficients (PCC) 0.71 \pm 0.03, 0.54 \pm 0.03 and 0.33 \pm 0.02 for LysoTracker, MitoTracker and ERTracker, respectively [36].

Reactive oxygen species production after Pc13 photoactivation

Photosensitizers, activated by absorption of visible light, initially form an excited singlet state, followed by transition to a long-lived excited triplet state. This triplet state can undergo photochemical reactions in the presence of oxygen to form ROS that can destroy cancer cells [33].

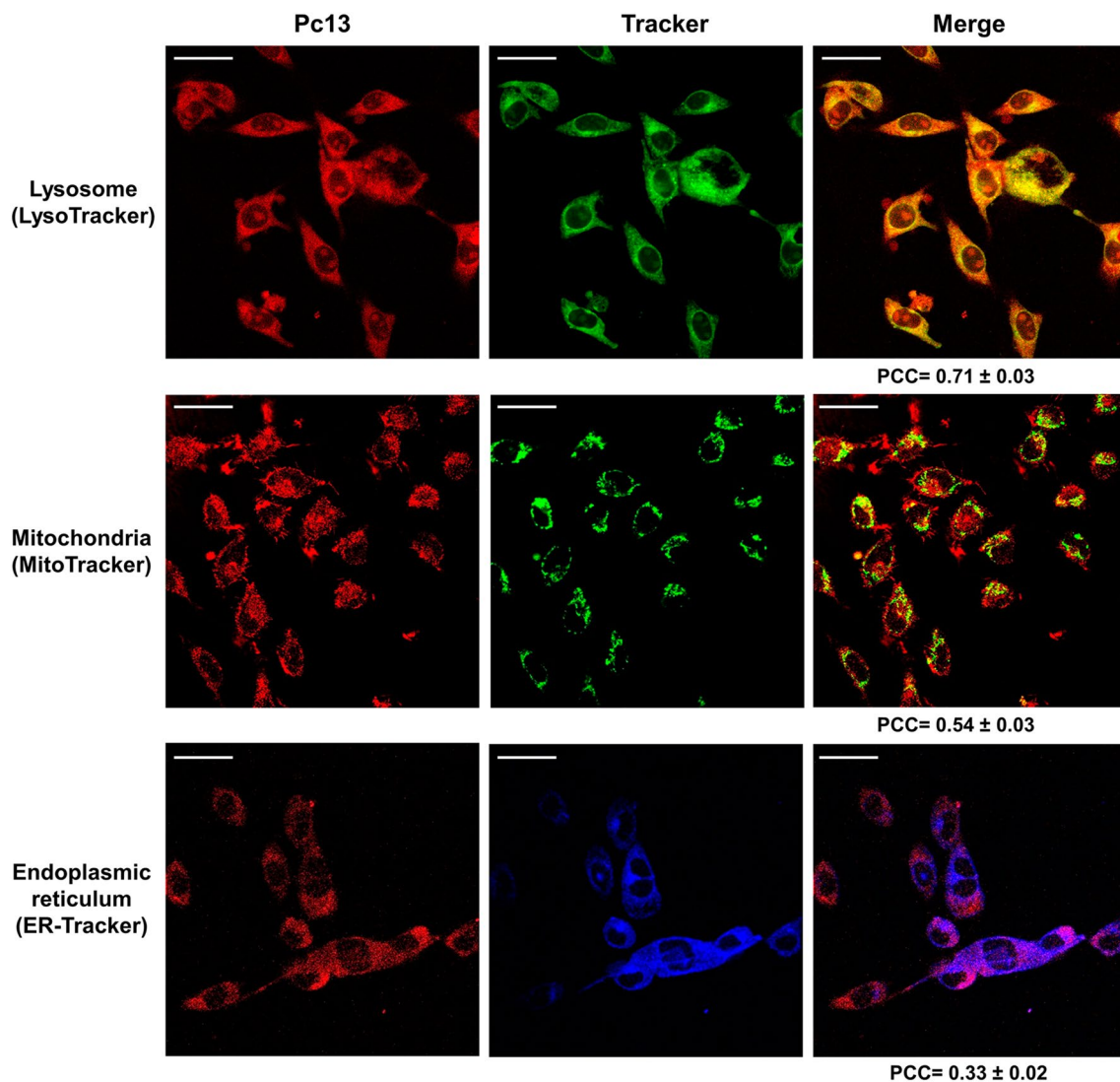


Fig. 2 Intracellular localization of Pc13. Melanoma B16F0 cells incubated with 5 μ M of Pc13 in the dark for 24 h were stained with LysoTracker Green DND-26 (100 nM, 45 min), MitoTracker Green FM (100 nM, 45 min) or ERTracker (1 μ M, 1 h). Fluorescence, examined by confocal microscopy Olympus FV 300, corresponds to Pc13

(red), lysosomes or mitochondria (green) and ER (blue). Overlays of the fluorescence images corresponding to Pc13 and trackers for each organelle and the corresponding Pearson's correlation coefficient (PCC) are shown. Scale bar: 40 μ m. (Color figure online)

ROS levels upon irradiation of Pc13-loaded B16F0 cells were evaluated using the probe DCFH-DA. A dose-dependent increase in the number of fluorescent cells corresponding to oxidized dichlorofluorescein was observed immediately after irradiation by fluorescence microscopy (Fig. 3a) and a significant increment of ROS levels per cell was quantitatively determined employing a fluorometer (Fig. 3b). When B16F0 cells were pre-incubated with a 5 mM solution of the antioxidant trolox, a complete protection from Pc13 phototoxicity was achieved (Fig. 3c), demonstrating that ROS are crucial mediators in the mechanism of cell death triggered by Pc13.

Modes of cell death triggered by Pc13 irradiation

In order to characterize the mechanisms of cell death induced by Pc13 PDT, cell morphology was initially evaluated after acridine orange (AO) and ethidium bromide (EB) staining. AO is a vital dye that stains both live and dead cells and EB stains only cells that have lost membrane integrity [37, 38]. While control B16F0 cells had uniform green fluorescence, the presence of cells with apoptotic characteristics, including blebbing, shrinking and bright green staining as a consequence of chromatin condensation, was observed after irradiation of cells treated with 0.2 μ M

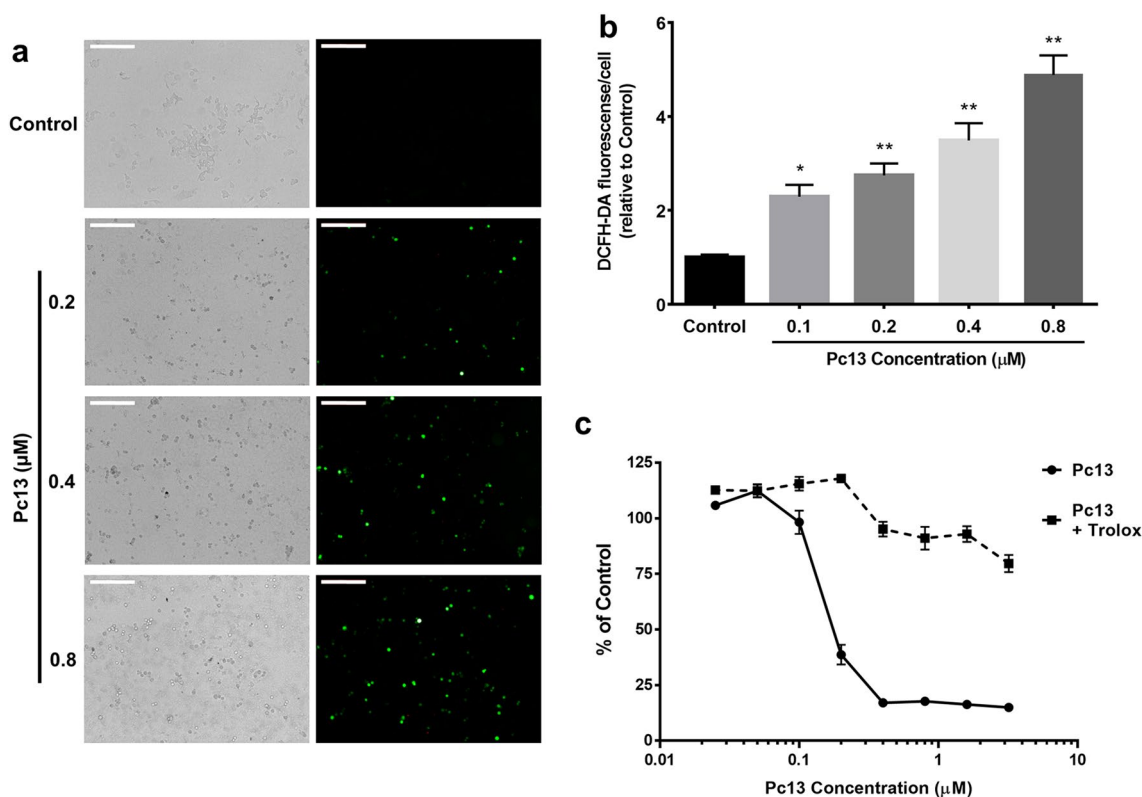


Fig. 3 Intracellular ROS production after Pc13 PDT. **a** B16F0 cells plated on coverslips were incubated with different concentrations of Pc13 and then irradiated with a light dose of 340 mJ cm^{-2} . ROS content was evidenced using the probe DCFH-DA (10 μM). Immediately post-irradiation, DCF fluorescence was detected in a Leica DM2000 fluorescence microscope, scale bar: 200 μm . **b** B16F0 cells plated in 6-well microplates were incubated with different concentrations of Pc13 and irradiated. DCF green fluorescence was measured in cell lysates with a Jasco FP-6500 fluorometer (excitation: 485 nm , emission: 530 nm). Results are expressed as DCF fluorescence per

cell, relative to control. Total viable cell number was determined by Trypan blue exclusion method. Results correspond to mean \pm SEM, $n=6$. ANOVA-Dunnet * $p<0.05$, ** $p<0.01$, significantly different from cells incubated in the absence of Pc13. **c** B16F0 cells incubated with different concentrations of Pc13 were pre-treated for 1 h with 5 mM of the antioxidant trolox and 24 h post-irradiation, phototoxicity was evaluated by Hexosaminidase method. Results are expressed relative to control obtained in the absence of Pc13 and represent the mean \pm SEM of three different experiments

Pc13 (Fig. 4a, b). Thus, 25% of early apoptotic cells were quantified immediately post irradiation, and this percentage decreased at 1 h and 3 h p.i., whereas the population of cells in late apoptosis, which incorporated EB and therefore stained orange but maintained apoptotic nuclei, increased to 20% after 3 h of irradiation. Nuclear condensation as a result of Pc13 photoactivation was also observed by Hoechst staining (Fig. 4a). Simultaneously, a significant increment of orange necrotic cells with no condensed chromatin was identified after irradiation, reaching approximately 40% at 3 h p.i (Fig. 4a, b). When irradiation of Pc13-treated B16F0 cells was performed in the presence of trolox, cell morphology and staining were similar to control cells (Fig. 4c), indicating that ROS are responsible for the induction of morphological changes mediated by Pc13 irradiation.

As shown in Fig. 4c, the phototoxic effect of Pc13 also led to a marked reduction of orange staining of acidic

organelles, an event characteristic of lysosomal membrane permeabilization (LMP) [39]. The loss of a punctuate pattern of staining obtained with LysoTracker Green probe and the presence of a lysosomal protease, such as cathepsin D, in cytosol after Pc13-treated cells irradiation is evidence that supports disruptions in lysosomes structure (Online Resource 2).

B16F0 cells also showed alterations of cell cycle phase distribution and DNA content after Pc13 PDT. A significant reduction of cells in S phase associated with an increase of cells in G_0/G_1 phase was shown by flow cytometry analysis of propidium iodide stained cells (Fig. 5a). Moreover, an increment in the proportion of hypodiploid cells was observed 1 h after irradiation ($21 \pm 8\%$ treated vs $5 \pm 2\%$ control) and maintained up to 3 h p.i. (Fig. 5b), consistent with the induction of an apoptotic response.

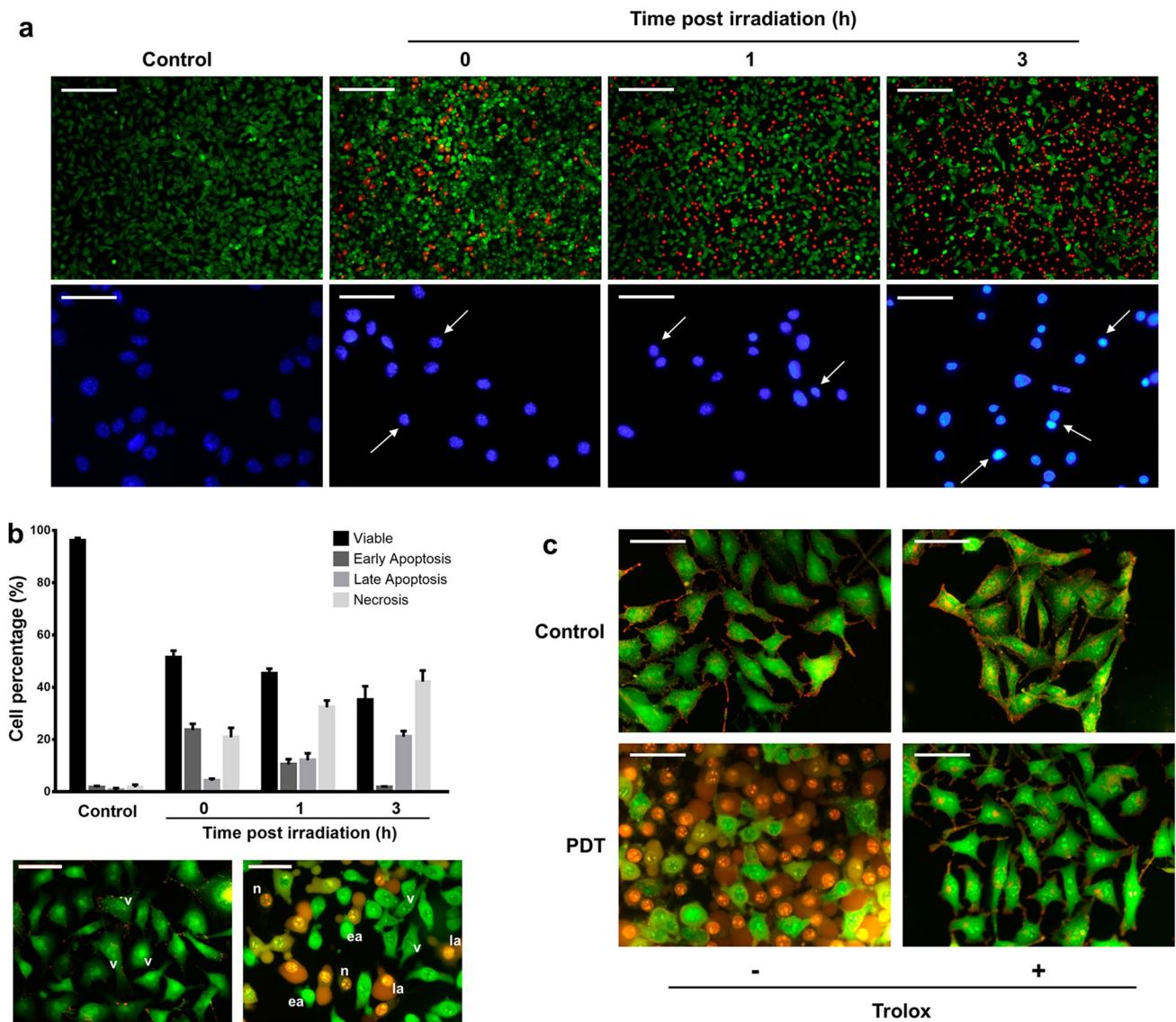


Fig. 4 Cell morphology modifications triggered after irradiation of Pc13-treated cells. **a** B16F0 cells grown on coverslips were incubated with 0.2 μM of Pc13 in the dark. Then, cells were irradiated (340 mJ cm^{-2}) and stained with acridine orange/ethidium bromide (upper panel, scale bar: $200 \mu\text{m}$) or Hoechst 33258 (lower panel, scale bar: $50 \mu\text{m}$) at different times post irradiation. Cell and nuclear morphology was examined in a Leica DM2000 fluorescence microscope. Arrows indicate condensed nuclei. **b** The percentage of different cellular populations was determined by manual counting of $\times 40$

fluorescence images, considering (v) viable, (ea) early apoptotic, (la) late apoptotic and (n) necrotic cells. Representative images of control and Pc13-treated cells ($0.2 \mu\text{M}$) stained at time 0 post irradiation are shown. **c** B16F0 cells incubated with $0.2 \mu\text{M}$ Pc13 were irradiated (340 mJ cm^{-2}) in the absence or presence of 5 mM trolox. Fluorescence images obtained 1 h p.i. after acridine orange/ethidium bromide staining are shown. Orange punctuate corresponds to acidic organelles. Scale bar: $50 \mu\text{m}$. (Color figure online)

Determination of necrosis after Pc13 PDT

Necrosis is a type of cell death characterized by plasma membrane rupture. Loss of cell membrane integrity results in the release of the cytoplasmic contents into the surrounding medium [35]. Thus, necrotic cell death was further evaluated by LDH determination in culture supernatants from control and treated cells. As shown in Fig. 6a, LDH activity in the extracellular medium from B16F0 cells treated

with $0.2 \mu\text{M}$ Pc13 significantly increased immediately after irradiation with 340 mJ cm^{-2} , reaching 45% of necrosis at 3 h p.i. Furthermore, increasing Pc13 concentrations and/or light doses produced higher LDH release at 0 h p.i., suggesting that necrotic response could be modulated by the overall PDT dose (Fig. 6b). This finding was confirmed by the increment in cell population that incorporated ethidium bromide dye when higher light dose (680 mJ cm^{-2}) or Pc13 concentration (up to $1 \mu\text{M}$) were employed (Fig. 6c). The

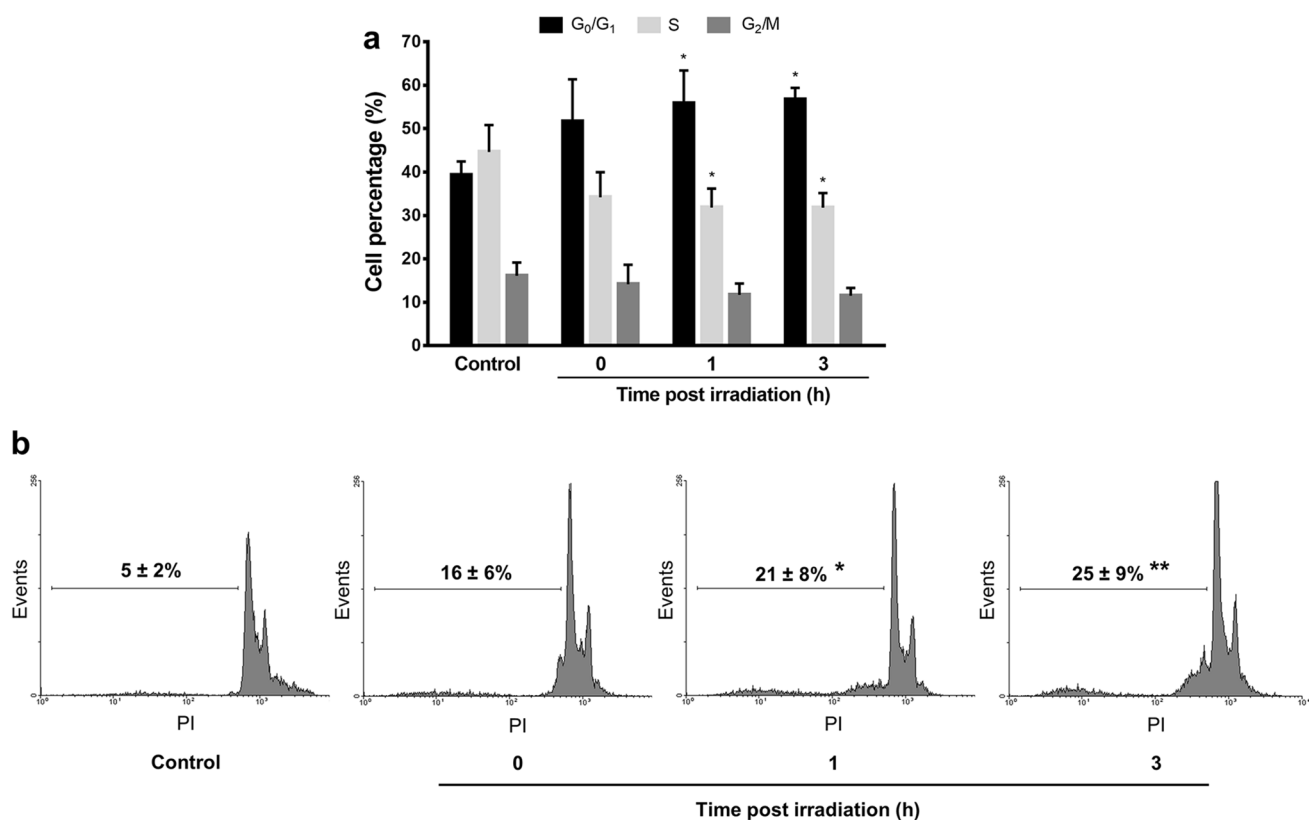


Fig. 5 Effect of Pc13 irradiation on cell cycle and DNA content. **a** Pc13-treated B16F0 cells were fixed at different times post irradiation and then stained with propidium iodide (PI) and analyzed in a FAC-SCalibur flow cytometer. Populations in each phase of the cell cycle were determined using Cylchred software. **b** DNA content was also

analyzed using WinMDI 2.8 software and the percentage of hypodiploid cells was obtained. Representative histograms of each condition are shown. Experiments were performed in triplicate and results correspond to mean ± SEM ANOVA-Dunnet * $p < 0.05$, ** $p < 0.01$, respect to non-treated cells

simultaneous rise of both parameters produced an almost complete induction of necrosis immediately after irradiation (Fig. 6c).

Pc13 irradiation activates the intrinsic apoptotic pathway

In order to further investigate the underlying mechanisms of Pc13 phototoxicity, we examined the possible alterations in the expression levels of Bcl-2 family proteins. These proteins are critical regulators of the mitochondrial outer membrane integrity and thereby a misbalance in their expression determines the cellular commitment to apoptosis [40]. As shown in Fig. 7a an early decrease of the anti-apoptotic proteins Bcl-2 and Bcl-xL was detected after irradiation of Pc13-treated cells. Although the expression of the proapoptotic protein Bax was not affected by Pc13 photoactivation, the cleavage of Bid was observed immediately post irradiation (Fig. 7a). Therefore, we next evaluated whether Pc13 irradiation caused alterations in mitochondrial transmembrane potential ($\Delta\psi_m$) in melanoma cells using the

cell membrane permeable - $\Delta\psi_m$ -sensitive - fluorescent dye DiOC₆. A reduction in green fluorescence in PDT-treated cells, observed by microscopy, and an increase in the population of cells with reduced DiOC₆ intensity, evidenced by flow cytometry at time 0 (74 ± 9% vs 15 ± 9%) and 1 h post irradiation (65 ± 8% vs 15 ± 9%), revealed that Pc13 PDT triggered a rapid decrease in $\Delta\psi_m$ (Fig. 7b). Accordingly, the presence of mitochondrial cytochrome *c* in the cytosolic fraction was detected at the same time after irradiation (Fig. 7c). The release of cytochrome *c* to cytosol as a result of mitochondrial membrane permeabilization is followed by the formation of the apoptosome, a large caspase-activating complex, corresponding to the intrinsic apoptotic pathway [41]. In this sense, the activation of procaspase-3 through proteolytic cleavage was shown by the zymogen reduction in western blot assay (Fig. 8a). Furthermore, a significant increase of caspase-3 activity was evidenced in Pc13-treated cells at 1 h and 3 h post irradiation, employing the fluorogenic substrate DEVD-AMC (Fig. 8b). The decrease of the 116 kDa caspase-3 substrate PARP-1, and the appearance of a 89 kDa fragment suggested PARP-1 cleavage by caspase-3

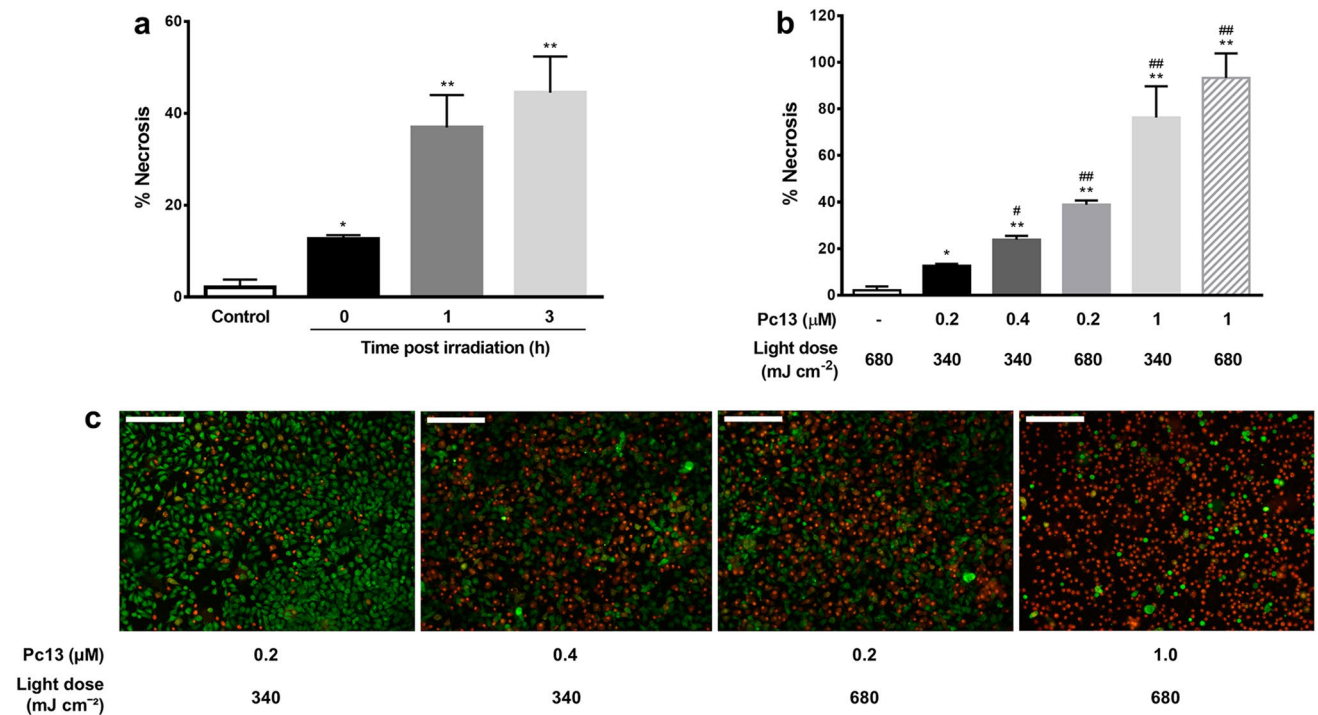


Fig. 6 Plasma membrane permeabilization after Pc13 photoactivation. **a** After incubation of B16F0 cells in the absence or presence of 0.2 μM of Pc13 for 24 h and irradiation with a light dose of 340 mJ cm^{-2} , permeabilization of plasma membrane was evaluated by measuring LDH activity in aliquots (20 μl) of culture supernatants at different times post irradiation. **b** B16F0 cells were incubated with increasing concentration of Pc13 and then irradiated with 340 or 680 mJ cm^{-2} . LDH activity was assessed at time 0 post irradiation.

Results are expressed as % necrosis respect to maximum lysis treatment obtained in Triton X-100 1% for 1 h and correspond to mean \pm SEM ANOVA-Dunnet * $p < 0.05$, ** $p < 0.01$, significantly different from cells incubated in the absence of Pc13, # $p < 0.05$, ### $p < 0.01$, significantly different from cells treated with 0.2 μM Pc13 and irradiated with 340 mJ cm^{-2} . **c** Cell morphology was analyzed by fluorescence microscopy after acridine orange/ethidium bromide staining in some phototoxic conditions at 0 h p.i. Scale bar: 200 μm

after PDT treatment (Fig. 8c). Incubation of B16F0 cells with the pan-caspase inhibitor Z-VAD-FMK before irradiation partially reduced phototoxicity when moderate doses of PDT were employed (0.1–0.2 μM Pc13, 340 mJ cm^{-2}), indicating the critical role of the apoptotic pathway in Pc13 phototoxic action (Fig. 8d).

Discussion

Photodynamic therapy is a treatment modality that has been assayed for non-malignant diseases and for many types of cancers. However, melanoma showed resistance towards PDT employing hematoporphyrin derivatives, such as Photofrin, due to the presence of melanin pigment that competed with the photosensitizer for the absorption of photons [42]. Melanin could also function as a ROS scavenger and may have antioxidant effect, leading to disruption of PDT-induced apoptotic pathways and tumour development [43, 44]. Thus, the synthesis and characterization of new photosensitizers absorbing in the 700–800 nm near infrared spectral region, where the absorption of melanin is minimal, and

that can overcome this PDT resistance are being explored. Phthalocyanines were identified in a recent work as the most efficient photosensitizers, when a group of four porphyrins and six phthalocyanines were assayed in WM35 melanoma cells [45]. In this study we demonstrated the efficacy of Pc13 phototoxicity in various cell lines, including pigmented and non-pigmented melanomas, indicating that PS absorption was not interfered by melanin. In fact, pigmented cells, such as B16F0 and B16F10 were more sensitive to Pc13 PDT (IC_{50} 0.20 and 0.45 μM respectively) than non-pigmented A375 cells (IC_{50} 3.6 μM), suggesting that melanin could play a role in Pc13 photodamage. In this sense, Davis and coworkers [26] showed that hypericin-induced ROS increased permeability of melanosomes, which led to cell death as a result of the release of toxic melanin precursors to the cytoplasm.

Resistance to agents recently approved for the treatment of melanoma has been described. In particular, the benefit of BRAF inhibitors (e.g. vemurafenib and dabrafenib) is limited by the frequent and rapid onset of resistance [46]. Our results demonstrated that Pc13 irradiation induced both wild type (B16F0, B16F10) and BRAF mutated (M1/15, WM35,

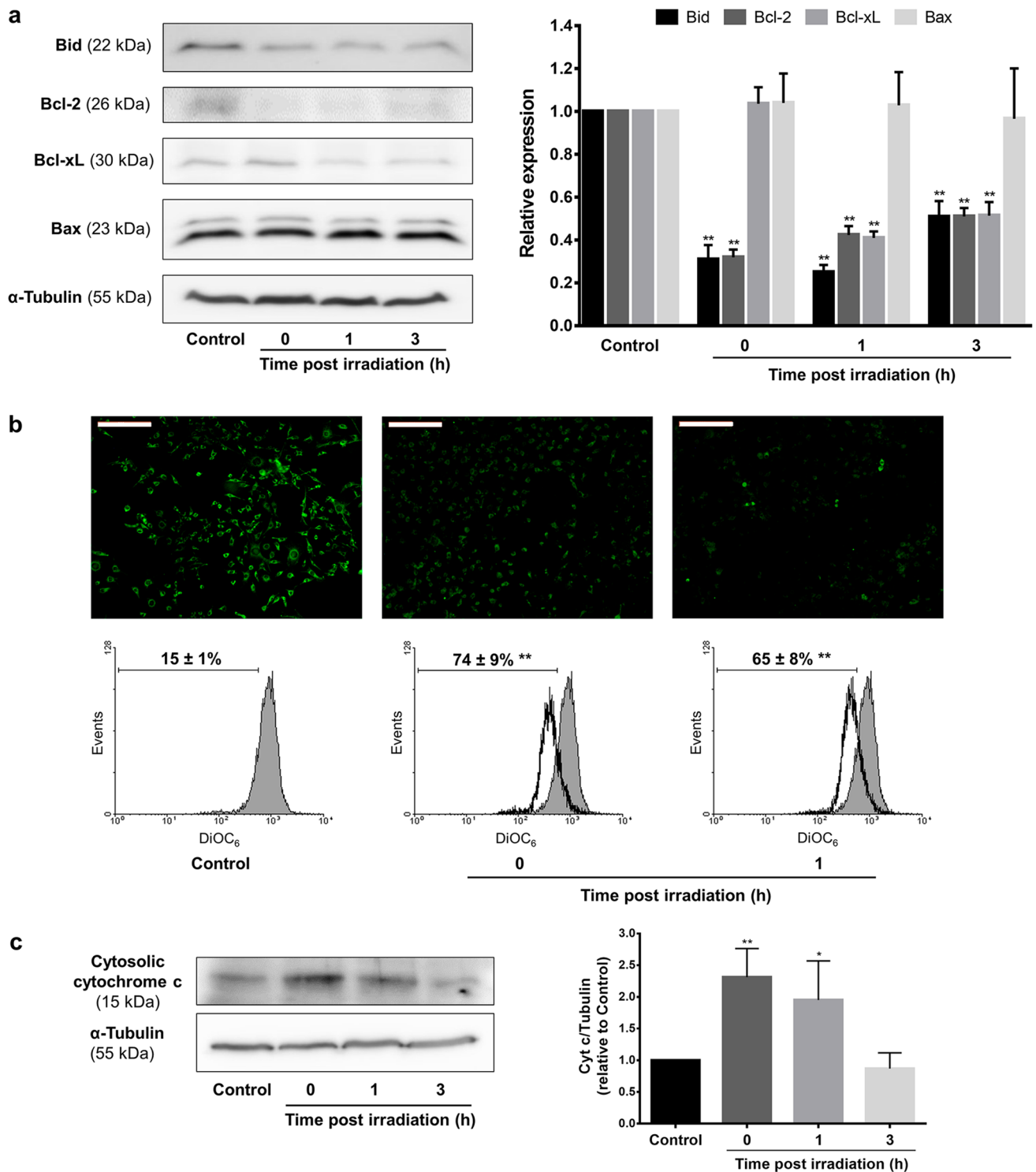


Fig. 7 Changes in Bcl-2 family proteins levels and mitochondrial outer membrane depolarization induced by Pc13 PDT. **a** B16F0 cells treated with 0.2 μ M of Pc13 were exposed to a light dose of 340 mJ cm^{-2} and incubated for different time-periods. Then, cell lysates (50 $\mu\text{g/lane}$) were submitted to western blot assays. **b** Pc13-loaded and irradiated B16F0 cells were stained with DiOC₆ and visualized with a Leica DM2000 fluorescence microscope (ex: 470–490 nm, em: 515 nm), scale bar: 200 μm (upper panel) or analyzed using a FACS Calibur flow cytometer (lower panel). The percentage

of cells with mitochondrial membrane depolarization is indicated; **c** Protein expression levels of cytochrome *c* were detected in cytosolic fractions obtained after irradiation of B16F0 cells exposed to 0.2 μM of Pc13. For western Blot assays, results from one representative experiment are shown (left panels). α -Tubulin was used as loading control. Densitometric analyses correspond to mean \pm SEM of three different experiments (right panels). ANOVA-Dunnett * $p < 0.05$, ** $p < 0.01$, significantly different from control (irradiated cells without Pc13)

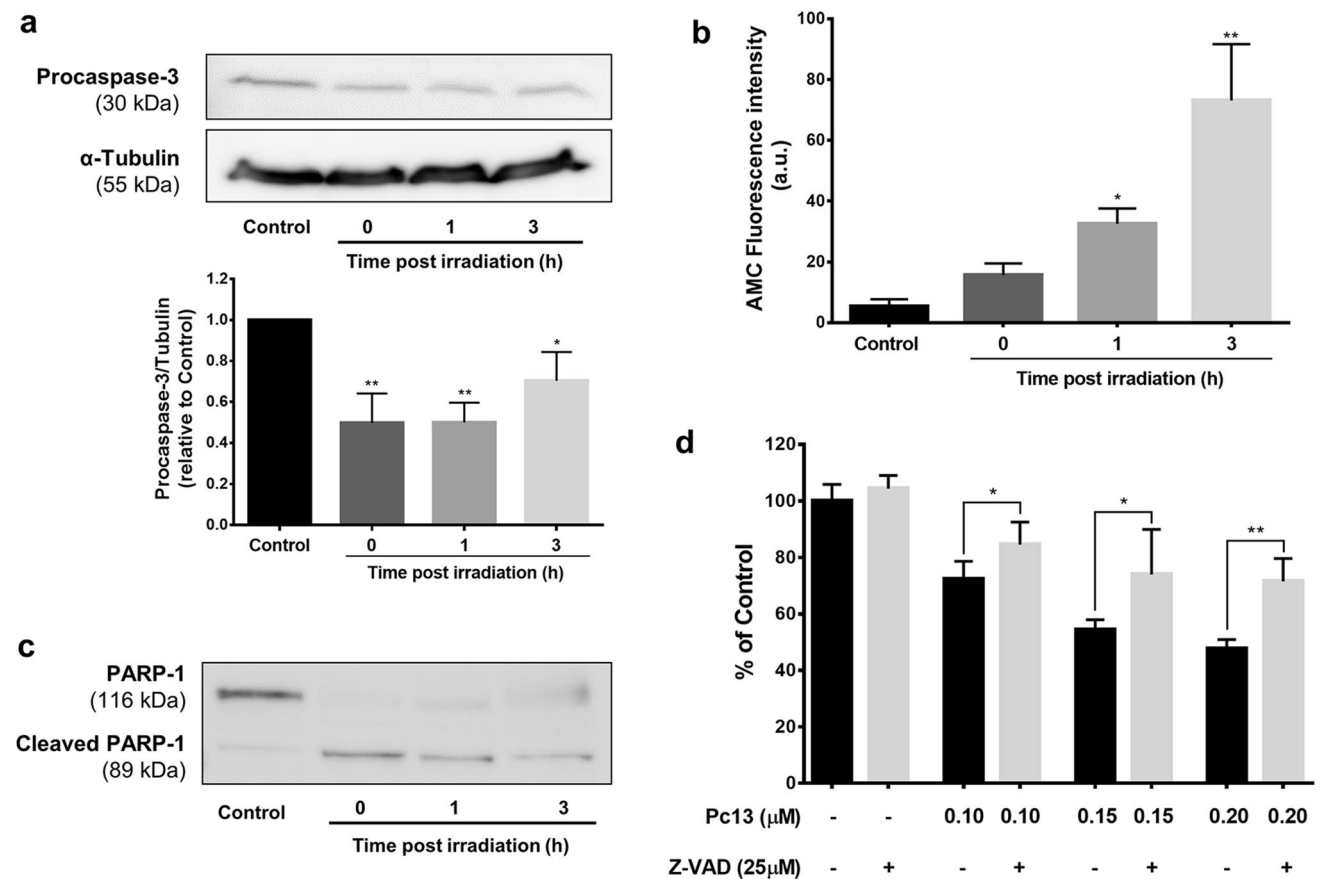


Fig. 8 Caspase-3 activation after Pc13 irradiation in B16F0 cells. **a** Western blot assay of procaspase-3 detected in cell lysates ($50\ \mu\text{g}/\text{lane}$) obtained after irradiation ($340\ \text{mJ cm}^{-2}$) of B16F0 cells exposed to $0.2\ \mu\text{M}$ Pc13. Results from one representative experiment are shown (upper panel). α -Tubulin was used as loading control. Densitometric analysis (lower panel). **b** Caspase-3 activity was determined at different times post irradiation using the fluorogenic substrate Ac-

DEVD-AMC. **c** Western blot analysis of PARP-1 (116 kDa) cleavage after PDT in B16F0 cells. PARP-1 fragment (89 kDa) was detected at different times post irradiation. **d** Pc13-treated B16F0 cells were pre-incubated 1 h before irradiation with $25\ \mu\text{M}$ of Z-VAD-FMK and 24 h p.i. phototoxicity was evaluated by Hexosaminidase method. Results correspond to mean \pm SEM of at least three different experiments. ANOVA-Dunnett * $p < 0.05$, ** $p < 0.01$

A375) cell death and thus phototoxicity does not depend on tumour cell genomic characteristics. An additional advantage of this type of PS is the absorption of light in the far-red region of the spectrum, a feature that allows the photoactivation in deeper tissues and might be clinically relevant.

We further explored the mechanisms involved in Pc13 PDT-mediated cell death in B16F0 cells, the most sensitive melanoma cell line assayed. Results showed that irradiation led to an increase in the intracellular levels of ROS and that the addition of the antioxidant agent trolox completely abolished phototoxic action of Pc13, demonstrating the essential role of the oxidative stress in the Pc13 PDT-induced cell death. Then, we evaluated Pc13 subcellular localization, a factor that strongly affects PDT activity [14, 47]. The location of the PS determines which cellular targets would be damaged and the mechanisms of cell death that would be triggered [48–51]. In a previous study we observed the preferential accumulation of Pc13 in lysosomes of human

nasopharynx carcinoma KB cells [31], as it was shown for others cationic PS, such as cationic porphyrins [52]. However, several authors have established that positively charged dyes could be electrophoretic driven to mitochondria and accumulate at these organelles [47, 53, 54]. By confocal microscopy we observed that Pc13 localizes both in lysosomes and mitochondria of B16F0 melanoma cells. Mitochondria targeting is considered particularly important for an effective anti-cancer therapy, since it may induce a rapid apoptotic response [55, 56]. According to this, our results demonstrated the decrease of $\Delta\psi_m$ at time 0 post irradiation, which led to cytochrome *c* release to cytosol. In addition, changes in the expression levels of Bcl-2 family proteins were triggered after Pc13 photoactivation and this may facilitate mitochondrial membrane permeabilization [40]. A drastic decrease of antiapoptotic Bcl-2 and Bcl-xL and the cleavage of Bid were shown in the present study, whereas no Bax modification was evidenced. Although

selective and direct photodamage to the Bcl-2 family proteins by photosensitizers has been proposed [57, 58], in a previous work with KB cells we demonstrated the role of lysosomal cathepsin D in the cleavage of Bid [34]. Accordingly, since Pc13 also localizes in lysosomes of B16F0 cells, we herein observed lysosomal membrane permeabilization (LMP), suggesting a potential role of both ROS and lysosomal proteases in Bcl-2 family proteins reduction.

The induction of an apoptotic program of cell death by Pc13 irradiation was further evidenced by the rapid activation of caspase-3 and the cleavage of one of its substrates PARP-1, leading to nuclei signs of fragmentation and condensed chromatin. Taking into account that caspase inhibitor Z-VAD-FMK only partially prevented phototoxic action of Pc13, the involvement of a caspase-independent pathway of cell death was proposed. In this sense, it has been reported that PDT can result in both apoptosis and necrosis [26, 59, 60]. In order to explore the induction of a necrotic process after Pc13 treatment, we studied the effect of Pc13 photoactivation on B16F0 cells plasma membrane integrity. The increase in LDH enzymatic activity in the extracellular medium and ethidium bromide uptake after irradiation of Pc13-treated cells were indicative of necrosis. Our results also showed that the extent of cell death by necrosis could be modulated by Pc13 concentration and/or light dose employed. It has been described that the response to PDT may vary with respect to not only total PS and light delivered, but also the cell type, the photosensitizer used and its intracellular localization [61–63]. In this regard, it was shown that a Gallium phthalocyanine in combination with metformin induced apoptosis in metastatic M1/15 cells and necrosis in WM35 cell line [30]. Concerning PS subcellular localization, Fabris et al. [58] determined that necrosis represented the prevailing mode of death of transformed fibroblasts incubated with a Zn(II) phthalocyanine mainly localized in the plasma membrane, whereas morphological changes typical of apoptosis were revealed when this Pc was found in mitochondria.

Studies reported here indicate that both apoptosis and necrosis were triggered when IC₅₀ of Pc13 was employed, being the proportion of necrotic cell death increased at higher doses of PDT. The activation of multiple cell death pathways by Pc13 irradiation would overcome the problem of apoptosis resistance, a common mechanism of tumour progression and cancer therapeutics failure [15, 64]. Furthermore, the induction of a necrotic process could trigger an inflammatory reaction, leading to development of systemic immunity [13, 65]. It has been described that PDT produces an acute inflammation that attracts leukocytes to treated tumours by exposing or creating new antigens, and by inducing heat-shock proteins that enhance the efficiency of antigen cross-presentation to form more effective tumour-specific cytotoxic T cells [18]. The immune reaction elicited

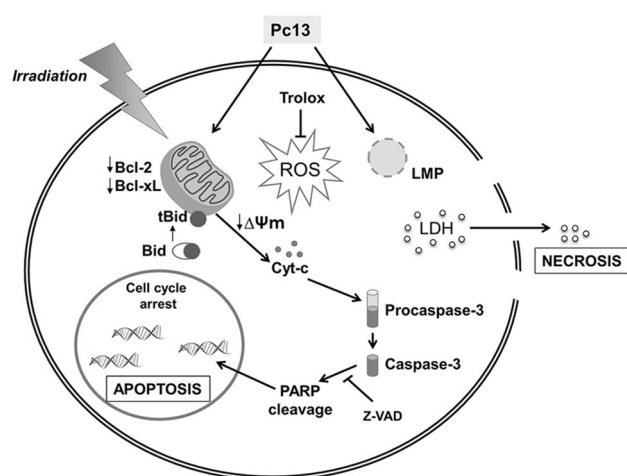


Fig. 9 Modes of cells death triggered by Pc13 irradiation in B16F0 cells. The formation of ROS after irradiation in the primary sites of Pc13 accumulation leads to lysosomal membrane permeabilization (LMP), mitochondrial outer membrane depolarization, cytochrome *c* release to cytosol and activation of caspase-3, hallmarks of an apoptotic response. In addition, the release of cytosolic LDH to the extracellular medium indicates plasma membrane alteration as a result of cell death by necrosis

by the photoinduced necrosis could offer a better control of cell growth in metastatic tumours [59, 66]. Although typical signs of apoptosis and necrosis were identified in this study, the contribution of other modes of cell death induced by Pc13 PDT, such as autophagy or paraptosis, can not be discarded [51].

In summary, results obtained demonstrate that Pc13 photoactivation produces an increase in the level of ROS, which elicits a cytotoxic response. The oxidative stress triggers lysosomal membrane permeabilization, decrease of anti-apoptotic proteins, cleavage of Bid and the consequent reduction of mitochondrial membrane potential. The release of cytochrome *c* to cytosol initiates the intrinsic apoptotic pathway, which finally activates caspase-3, leading to cleavage of PARP-1 and DNA fragmentation. On the other hand, oxidative response induces alterations in plasma membrane, characteristic of necrosis, promoting the release of cytosolic content to extracellular medium (Fig. 9). Thus, considering that Pc13 PDT activates both apoptotic and necrotic cell death in B16F0 cells, we suggest that Pc13 represents a promising alternative for melanoma treatment, which could exert direct cytotoxic effects on tumour cells and also cause a systemic anti-tumour response. Although the penetration of light into a relatively opaque tissue like melanoma might be limited, Pc13 PDT could be useful for destruction of malignant cells in situ at surgical margins and also for activating a systemic immune response against tumor antigens. To explore Pc13 PDT efficacy in vivo, further studies will be performed in mouse melanoma models.

Acknowledgements This work was supported by grants of Agencia Nacional de Promoción Científica y Tecnológica PICT 2013-0144, Consejo Nacional de Investigaciones Científicas y Técnicas PIP 0154 and Secretaria de Ciencia y Técnica de la Universidad de Buenos Aires (UBACyT 20020130100024), Argentina. Authors are grateful to Dr. Marcela Villaverde for the generous gift of A375 cells.

Compliance with ethical standards

Conflict of interest The authors declare that they have no conflict of interest.

References

1. Fecher LA, Cummings SD, Keefe MJ, Alani RM (2007) Toward a molecular classification of melanoma. *J Clin Oncol* 25(12):1606–1620
2. Ferlay J, Soerjomataram I, Dikshit R, Eser S, Mathers C, Rebelo M, Parkin DM, Forman D, Bray F (2015) Cancer incidence and mortality worldwide: sources, methods and major patterns in GLOBOCAN 2012. *Int J Cancer* 136(5):E359–E386
3. Ossio R, Roldán-Marín R, Martínez-Said H, Adams DJ, Robles-Espinoza CD (2017) Melanoma: a global perspective. *Nat Rev Cancer* 17(7):393–394
4. Davies H, Bignell GR, Cox C, Stephens P, Edkins S, Clegg S, Teague J, Woffendin H, Garnett MJ, Bottomley W, Davis N, Dicks E, Ewing R, Floyd Y, Gray K, Hall S, Hawes R, Hughes J, Kosmidou V, Menzies A, Mould C, Parker A, Stevens C, Watt S, Hooper S, Wilson R, Jayatilake H, Gusterson BA, Cooper C, Shipley J, Hargrave D, Pritchard-Jones K, Maitland N, Chenevix-Trench G, Riggins GJ, Bigner DD, Palmieri G, Cossu A, Flanagan A, Nicholson A, Ho JW, Leung SY, Yuen ST, Weber BL, Seigler HF, Darrow TL, Paterson H, Marais R, Marshall CJ, Wooster R, Stratton MR, Futreal PA (2002) Mutations of the BRAF gene in human cancer. *Nature* 417(6892):949–954
5. Rajkumar S, Watson IR (2016) Molecular characterisation of cutaneous melanoma: creating a framework for targeted and immune therapies. *Br J Cancer* 115(2):145–155
6. Bollag G, Hirth P, Tsai J, Zhang J, Ibrahim PN, Cho H, Spevak W, Zhang C, Zhang Y, Habets G, Burton EA, Wong B, Tsang G, West BL, Powell B, Shellooe R, Marimuthu A, Nguyen H, Zhang KY, Artis DR, Schlessinger J, Su F, Higgins B, Iyer R, D'Andrea K, Koehler A, Stumm M, Lin PS, Lee RJ, Grippo J, Puzanov I, Kim KB, Ribas A, McArthur GA, Sosman JA, Chapman PB, Flaherty KT, Xu X, Nathanson KL, Nolop K (2010) Clinical efficacy of a RAF inhibitor needs broad target blockade in BRAF-mutant melanoma. *Nature* 467:596–599
7. Topalian SL, Hodi FS, Brahmer JR, Gettinger SN, Smith DC, McDermott DF, Powderly JD, Carvajal RD, Sosman JA, Atkins MB, Leming PD, Spigel DR, Antonia SJ, Horn L, Drake CG, Pardoll DM, Chen L, Sharfman WH, Anders RA, Taube JM, McMiller TL, Xu H, Korman AJ, Jure-Kunkel M, Agrawal S, McDonald D, Kollia GD, Gupta A, Wigginton JM, Sznol M (2012) Safety, activity, and immune correlates of anti-PD-1 antibody in cancer. *N Engl J Med* 366(26):2443–2454
8. Wong DJ, Ribas A (2016) Targeted therapy for melanoma. *Cancer Treat Res* 167:251–262
9. Curtin JA, Fridlyand J, Kageshita T, Patel HN, Busam KJ, Kutzner H, Cho KH, Aiba S, Bröcker EB, LeBoit PE, Pinkel D, Bastian BC (2005) Distinct sets of genetic alterations in melanoma. *N Engl J Med* 353(20):2135–2147
10. Chapman PB, Hauschild A, Robert C, Haanen JB, Ascierto P, Larkin J, Dummer R, Garbe C, Testori A, Maio M, Hogg D, Lorigan P, Lebbe C, Jouary T, Schadendorf D, Ribas A, O'Day SJ, Sosman JA, Kirkwood JM, Eggermont AM, Dreno B, Nolop K, Li J, Nelson B, Hou J, Lee RJ, Flaherty KT, McArthur GA (2011) BRIM-3 Study Group. Improved survival with vemurafenib in melanoma with BRAF V600E mutation. *N Engl J Med* 364(26):2507–2516
11. Hugo W, Zaretsky JM, Sun L, Song C, Moreno BH, Hu-Lieskovan S, Berent-Maoz B, Pang J, Chmielowski B, Cherry G, Seja E, Lomeli S, Kong X, Kelley MC, Sosman JA, Johnson DB, Ribas A, Lo RS (2016) Genomic and transcriptomic features of response to anti-PD-1 therapy in metastatic melanoma. *Cell* 165(1):35–44
12. Dougherty TJ, Gomer CJ, Henderson BW, Jori G, Kessel D, Korbelik M, Moan J, Peng Q (1998) Photodynamic therapy. *J Natl Cancer Inst* 90:889–905
13. Agostinis P, Berg K, Cengel KA, Foster TH, Girotti AW, Gollnick SO, Hahn SM, Hamblin MR, Juzeniene A, Kessel D, Korbelik M, Moan J, Mroz P, Nowis D, Piette J, Wilson BC, Golab J (2011) Photodynamic therapy of cancer: an update. *CA Cancer J Clin* 61(4):250–281
14. Castano AP, Demidova TN, Hamblin MR (2004) Mechanisms in photodynamic therapy. Part one: photosensitizers, photochemistry and cellular localization. *Photodiag Photodyn Ther* 1:279–293
15. van Straten D, Mashayekhi V, de Bruijn HS, Oliveira S, Robinson DJ (2017) Oncologic photodynamic therapy: basic principles, current clinical status and future directions. *Cancers* 9(2):1–54
16. Hasan T, Ortel B, Moor A, Pogue B (2003) Holland-Frei cancer medicine, eds Kufe, D. et al. Ch. 40 BC Decker, Inc., Hamilton, Ontario
17. Dolmans DE, Fukumura D, Jain RK (2003) Photodynamic therapy for cancer. *Nat Rev Cancer* 3(5):380–387
18. Castano AP, Mroz P, Hamblin MR (2006) Photodynamic therapy and anti-tumour immunity. *Nat Rev Cancer* 6:535–545
19. Dimofte A, Zhu TC, Hahn SM, Lustig RA (2002) In vivo light dosimetry for motexafin lutetium-mediated PDT of breast cancer. *Lasers Surg Med* 31:305–312
20. Rosenthal MA, Kavar B, Hill JS, Morgan DJ, Nation RL, Stylli SS, Basser RL, Uren S, Geldard H, Green MD, Kahl SB, Kaye AH (2001) Phase I and pharmacokinetic study of photodynamic therapy for high-grade gliomas using a novel boronated porphyrin. *J Clin Oncol* 19(2):519–524
21. Bown SG, Rogowska AZ, Whitelaw DE, Lees WR, Lovat LB, Ripley P, Jones L, Wyld P, Gillams A, Hatfield AWR (2002) Photodynamic therapy for cancer of the pancreas. *Gut* 50:549–557
22. Favilla I, Favilla ML, Gosbell AD, Barry WR, Ellims P, Hill JS, Byrne JR (1995) Photodynamic therapy: a 5-year study of its effectiveness in the treatment of posterior uveal melanoma, and evaluation of haematoporphyrin uptake and photocytotoxicity of melanoma cells in tissue culture. *Melanoma Res* 5(5):355–364
23. Sibata CH, Colussi VC, Oleinick NL, Kinsella TJ (2001) Photodynamic therapy in oncology. *Expert Opin Pharmacother* 6(6):917–927
24. Braathen LR, Szeimies RM, Basset-Seguín N et al (2007) Guidelines on the use of photodynamic therapy for nonmelanoma skin cancer: an international consensus. *International Society for Photodynamic Therapy in Dermatology, 2005. J Am Acad Dermatol* 56:125–143
25. Brown SB, Brown EA, Walker I (2004) The present and future role of photodynamic therapy in cancer treatment. *Lancet Oncol* 5(8):497–508
26. Davids LM, Kleemann B, Kacerovská D, Pizinger K, Kidson SH (2008) Hypericin phototoxicity induces different modes of cell death in melanoma and human skin cells. *J Photochem Photobiol B* 91(2–3):67–76
27. Wainwright M (2008) Photodynamic therapy: the development of new photosensitisers. *Anticancer Agents Med Chem* 8(3):280–291
28. O'Connor AE, Gallagher WM, Byrne AT (2009) Porphyrin and nonporphyrin photosensitizers in oncology: preclinical and

- clinical advances in photodynamic therapy. *Photochem Photobiol* 85:1053–1074
29. Mfouo-Tynga I, Abrahamse H (2015) Cell death pathways and phthalocyanine as an efficient agent for photodynamic cancer therapy. *Int J Mol Sci* 16(5):10228–10241
 30. Tudor D, Nenu I, Filip GA, Olteanu D, Cenariu M, Tabaran F, Ion RM, Gligor L, Baldea I (2017) Combined regimen of photodynamic therapy mediated by Gallium phthalocyanine chloride and Metformin enhances anti-melanoma efficacy. *PLoS ONE* 12(3):e0173241 (**eCollection 2017**)
 31. Marino J, García Vior MC, Dicelio LE, Roguin LP, Awruch J (2010) Photodynamic effects of isosteric water-soluble phthalocyanines on human nasopharynx KB carcinomacells. *Eur J Med Chem* 45:4129–4139
 32. Dysart JS, Patterson MS (2005) Characterization of photofrin photobleaching for singlet oxygen dose estimation during photodynamic therapy of mll cells in vitro. *Phys Med Biol* 50:2597–2616
 33. Abrahamse H, Hamblin MR (2016) New photosensitizers for photodynamic therapy. *Biochem J* 473(4):347–364
 34. Marino J, García Vior MC, Furmento VA, Blank VC, Awruch J, Roguin LP (2013) Lysosomal and mitochondrial permeabilization mediates zinc(II) cationic phthalocyanine phototoxicity. *Int J Biochem Cell Biol* 45(11):2553–2562
 35. Chan FK, Moriwaki K, De Rosa MJ (2013) Detection of necrosis by release of lactate dehydrogenase activity. *Methods Mol Biol* 979:65–70
 36. Adler J, Parmryd I (2010) Quantifying colocalization by correlation: the Pearson correlation coefficient is superior to the Mander's overlap coefficient. *Cytometry A* 77(8):733–742
 37. Kasibhatla S, Amarante-Mendes GP, Finucane D, Brunner T, Bossy-Wetzel E, Green DR (2006) Acridine orange/ethidium bromide (AO/EB) staining to detect apoptosis. *CSH Protoc.* <https://doi.org/10.1101/pdb.prot4493>
 38. Liu K, Liu PC, Liu R, Wu X (2015) Dual AO/EB staining to detect apoptosis in osteosarcoma cells compared with flow cytometry. *Med Sci Monit Basic Res* 21:15–20
 39. Kågedal K, Zhao M, Svensson I, Brunk UT (2001) Sphingosine-induced apoptosis is dependent on lysosomal proteases. *Biochem J* 359(Pt 2):335–343
 40. Martinou JC, Youle RJ (2011) Mitochondria in apoptosis: Bcl-2 family members and mitochondrial dynamics. *Dev Cell* 21(1):92–101
 41. Kim H, Du F, Fang M, Wang X (2005) Formation of apoptosome is initiated by cytochrome c-induced dATP hydrolysis and subsequent nucleotide exchange on Apaf-1. *Proc Natl Acad Sci USA* 102(49):17545–17550
 42. Huang YY, Vecchio D, Avci P, Yin R, Garcia-Diaz M, Hamblin MR (2013) Melanoma resistance to photodynamic therapy: new insights. *Biol Chem* 394(2):239–250
 43. Sharma KV, Bowers N, Davids LM (2011) Photodynamic therapy-induced killing is enhanced in depigmented metastatic melanoma cells. *Cell Biol Int* 35:939–944
 44. Suzukawa AA, Vieira A, Winnischofer SM, Scalfio AC, Di Mascio P, Da Costa Ferreira AM, Ravanat JL, De Luna Martins D, Rocha ME, Martinez GR (2012) Novel properties of melanins include promotion of DNA strand breaks, impairment of repair, and reduced ability to damage DNA after quenching of singlet oxygen. *Free Radic Biol Med* 52:1945–1953
 45. Baldea I, Ion RM, Olteanu DE, Nenu I, Tudor D, Filip AG (2015) Photodynamic therapy of melanoma using new, synthetic porphyrins and phthalocyanines as photosensitisers—a comparative study. *Clujul Med* 88(2):175–180
 46. Bucheit AD, Davies MA (2014) Emerging insights into resistance to BRAF inhibitors in melanoma. *Biochem Pharmacol* 87(3):381–389
 47. Lei W, Xie J, Hou Y, Jiang G, Zhang H, Wang P, Wang X, Zhang B (2010) Mitochondria-targeting properties and photodynamic activities of porphyrin derivatives bearing cationic pendant. *J Photochem Photobiol B* 98(2):167–171
 48. Kramer-Marek G, Serpa C, Szurko A, Widel M, Sochanik A, Sniectura M, Kus P, Nunes RM, Arnaut LG, Ratuszna A (2006) Spectroscopic properties and photodynamic effects of new lipophilic porphyrin derivatives: efficacy, localisation and cell death pathways. *J Photochem Photobiol B* 84(1):1–14
 49. Buytaert E, Dewaele M, Agostinis P (2007) Molecular effectors of multiple cell death pathways initiated by photodynamic therapy. *Biochim Biophys Acta* 1776(1):86–107
 50. Ezzeddine R, Al-Banaw A, Tovmasyan A, Craik JD, Batinic-Haberle I, Benov LT (2013) Effect of molecular characteristics on cellular uptake, subcellular localization, and phototoxicity of Zn(II) *N*-alkylpyridylporphyrins. *J Biol Chem* 288(51):36579–36588
 51. Kessel D, Oleinick NL (2018) Cell death pathways associated with photodynamic therapy: an update. *Photochem Photobiol* 94(2):213–218
 52. Ricchelli F, Franchi L, Miotto G, Borsetto L, Gobbo S, Nikolov P, Bommer JC, Reddi E (2005) Meso-substituted tetra-cationic porphyrins photosensitize the death of human fibrosarcoma cells via lysosomal targeting. *Int J Biochem Cell Biol* 37(2):306–319
 53. Engelmann FM, Rocha SV, Toma HE, Araki K, Baptista MS (2007) Determination of *n*-octanol/water partition and membrane binding of cationic porphyrins. *Int J Pharm* 329:12–18
 54. Perry SW, Norman JP, Barbieri J, Brown EB, Gelbard HA (2011) Mitochondrial membrane potential probes and the proton gradient: a practical usage guide. *Biotechniques* 50(2):98–115
 55. Kessel D, Luo YJ (1998) Mitochondrial photodamage and PDT-induced apoptosis. *Photochem Photobiol B* 42(2):89–95
 56. Oleinick NL, Morris RL, Belichenko I (2002) The role of apoptosis in response to photodynamic therapy: what, where, why, and how. *Photochem Photobiol Sci* 1(1):1–21
 57. Kessel D, Castelli M (2001) Evidence that bcl-2 is the target of three photosensitizers that induce a rapid apoptotic response. *Photochem Photobiol* 74(2):318–322
 58. Xue LY, Chiu SM, Oleinick NL (2001) Photochemical destruction of the Bcl-2 oncoprotein during photodynamic therapy with the phthalocyanine photosensitizer Pc 4. *Oncogene* 20(26):3420–3427
 59. Fabris C, Valduga G, Miotto G, Borsetto L, Jori G, Garbisa S, Reddi E (2001) Photosensitization with zinc (II) phthalocyanine as a switch in the decision between apoptosis and necrosis. *Cancer Res* 61(20):7495–7500
 60. Luo Y, Kessel D (1997) Initiation of apoptosis *versus* necrosis by photodynamic therapy with chloroaluminum phthalocyanine. *Photochem Photobiol* 66(4):479–483
 61. Nagata S, Obana A, Gohto Y, Nakajima S (2003) Necrotic and apoptotic cell death of human malignant melanoma cells following photodynamic therapy using an amphiphilic photosensitizer, ATX-S10(Na). *Lasers Surg Med* 33(1):64–70
 62. Oleinick NL, Nieminen AL, Chiu SM (2008) Cell killing by photodynamic therapy. In: Hamblin MR, Mroz P (eds) *Advances in photodynamic therapy: basic, translational and clinical*. Artech House, Boston, pp 115–133
 63. Sharma KV, Davids LM (2012) Hypericin-PDT-induced rapid necrotic death in human squamous cell carcinoma cultures after multiple treatment. *Cell Biol Int* 36(12):1261–1266
 64. Igney FH, Krammer PH (2002) Death and anti-death: tumour resistance to apoptosis. *Nat Rev Cancer* 4(2):77–88
 65. Garg AD, Krysko DV, Vandenabeele P, Agostinis P (2011) DAMPs and PDT-mediated photo-oxidative stress: exploring the unknown. *Photochem Photobiol Sci* 10(5):670–680
 66. Korbek M (1996) Induction of tumor immunity by photodynamic therapy. *J Clin Laser Med Surg* 14(5):329–334